Chapter 6

Analysis of pinned-pinned shallow connected arches

Synopsis

We study the behavior of two interconnected arches. The arches we are considering here are pinned at both ends, and they are connected to each other through their common pin joint. When the load-bearing arch deforms due to a transverse load on it, the other arch also deforms due to the moment transfer at the common pin joint. Based on the deformation and stability of these connected arches, we categorize their nature into four different groups: *switching and bistable* (SB), *switching and not-bistable* (SNB), *not-switching and bistable* (NSB), and *not-switching and not-bistable* (NSNB). We present a method to analyse and predict the nature of such connected arches when two pinned-pinned arches of any random shape are connected to each other.

6.1 Introduction

Two pinned-pinned arches, when connected through a common pin joint, can produce a flip-flop mechanism that can act both as sensor and actuator. The literature on the analysis and design of arches is limited to single arch with pinned or fixed boundary conditions. As per our knowledge, the literature on the connected arch, like the one shown in Fig. 1, has not yet been published. The analysis and design of such kind of serially interconnected pinned-pinned arches, but not necessarily the sine arches, is the focus of this chapter. It is noted that, in these kinds of serially connected arches, the deformation of one arch impacts the deformation of the other arch. It is due to the moment transfer that occurs at the common pin joint. Due to the same reason, the arches in the connected arch configuration act as torsional springs to each other, which stiffness depends on the arch geometry and its deformation. Therefore, the deformation of one arch is affected due to the presence of another arch. Due to the arch's inherent nonlinearity, the equivalent rotational spring stiffness also varies simultaneously, further affecting their deformation. Hence, the arches act as a nonlinear rotational spring to one another. Although there is literature on the analysis

of pinned-pinned arches with a torsional spring of constant stiffness attached to one end of the arch, this study focuses on arches with variable torsional stiffness at one end. By minimizing the total potential energy and the constraint equation at the common pin joint, we obtain the governing equations to analyse connected arches.

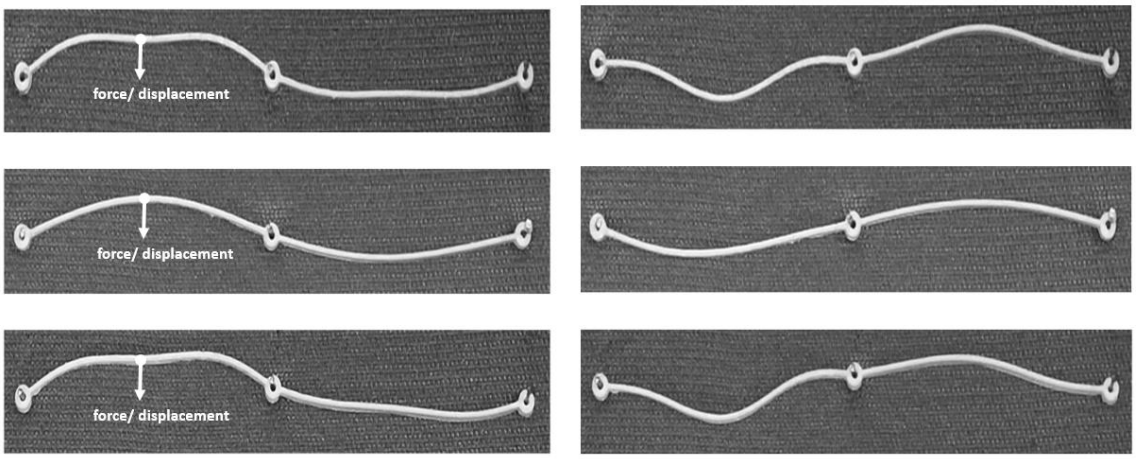

(a) Initial-profile or as-fabricated state (b) Toggle-profile or second stable state

Figure 6.1: 3D-printed connected arches showing the initial profile and their toggle profile. We apply force or displacement to the left arch as indicated by the downward arrow. When the force exceeds a threshold value, both the arches toggle to their inverted shape resulting in a flip-flop mechanism.

As we apply force to one of the arches, it starts deforming, which eventually deforms the other arch. With an increase in the displacement of the force value on the load-bearing arch, both the arches may flip to their inverted shape by changing their curvature, and if they retain their shape at their inverted shape even after the removal of load, they become bistable. Based on the switching and bistability of the configuration, we categorize connected arches into four different groups: switching and bistable (SB), switching and not-bistable (SNB), not-switching and bistable (NSB), and not-switching and not-bistable (NSNB). This nature of the connected arches depends on the arch geometry and hence on the individual torsional stiffness and torque-rotation characteristic. The main questions we address in this chapter are: (1) under what conditions would the second arch flip to its inverted shape and become bistable? and (2) under what conditions would the second arch flip to its inverted shape and become snap-through? In this chapter, we discuss the intriguing phenomena of connection between arch deformation and rotational stiffness by using the toque vs. rotation of the individual arch to predict the combined nature of two pinned-pinned arches of any random shape when they are connected to each other. The motivation behind studying the connected

arches is to design a fully mechanically operated self-offloading therapeutic footwear for diabetics and to design mechanical logic gates. A detailed discussion of these applications of connected arches will be covered in Chapter 8.

6.2 Analysis of connected arches

We take two arches of random shapes with pinned-pinned boundary conditions and connect them at a common revolute joint, as shown in Fig. 6.2. The span of the arch, L, the in-plane depth, d, the out-of-plane breadth, b, and the Young's modulus, E, are same for both the arches. The left-hand-side arch is called the load-bearing arch or $Arch_1$. The right-hand-side arch, which deforms only due to the deformation of $Arch_1$ is called $Arch_2$. In this chapter, we use subscript "1" for $Arch_1$ and subscript "2" for $Arch_2$ to express the energy terms. A transverse force f is applied to $Arch_1$ at its mid-span length, as shown in Fig. 6.2. We approximate the as-fabricated shape, $h_i(x)$, and the deformed shape, $w_i(x)$, of the arches by expressing them as a weighted linear combination of the mode weights of a straight pined-pinned column of length L, i.e.,

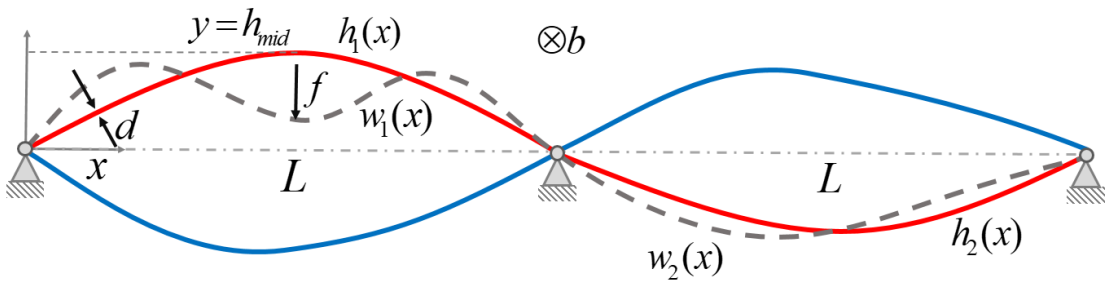

Figure 6.2: Connected pinned-pinned arches with all the dimensions showing the as-fabricated shape (red-solid), intermediate deformed shape (grey-dashed), and inverted stable shape (blue-solid).

$$
\begin{aligned}
h_1(x) &= h_{mid}\sum_{i=1}^{n} a_i\varphi_i \\
w_1(x) &= h_{mid}\sum_{i=1}^{n} A_i\varphi_i \\
h_2(x) &= h_{mid}\sum_{i=1}^{n} b_i\varphi_i \\
w_2(x) &= h_{mid}\sum_{i=1}^{n} B_i\varphi_i
\end{aligned}
\tag{6.1}
$$

where $\varphi_i = \sin\left(\frac{i\pi x}{L}\right)$ is the i^{th} mode shape of the straight column, a_is and b_is are the mode weights of φ_i at the as-fabricated stress-free states of $Arch_1$ and $Arch_2$, respectively. A_is and B_is are the mode weights of $Arch_1$ and $Arch_2$, respectively at their deformed states. The mid-span height of $Arch_1$ is h_{mid}, and n is the number of buckling mode shapes considered to approximate the as-fabricated and the deformed state of the arches.

We proceed with the analysis in a normalized framework to identify the geometric parameters that affect the nature of the connected arch. It is noted that all normalized parameters are denoted by upper-case symbols. To obtain the governing equations for the connected arch, we minimize the total potential energy with respect to the deformed mode weights of the arches. The total potential energy of the arch consists of strain energy due to bending (SE_b), strain energy due to axial compression (SE_c), and work potential (WP) due to the quasi-static load at the center of $Arch_1$.

The normalized as-fabricated shape, $H_i(X)$, and the normalized deformed profile, $W_i(X)$ of the arch is given by:

$$\begin{aligned} H_1(X) &= \sum_{i=1}^{n} a_i \varphi_i(X) \\ W_1(X) &= \sum_{i=1}^{n} A_i \varphi_i(X) \\ H_2(X) &= \sum_{i=1}^{n} b_i \varphi_i(X) \\ W_2(X) &= \sum_{i=1}^{n} B_i \varphi_i(X) \end{aligned} \tag{6.2}$$

where

$$X = \frac{x}{L} \quad H(X) = \frac{h(x)}{h_{mid}} \quad W(T,X) = \frac{w(t,x)}{h_{mid}} \quad h_{mid} = \sum_{i=1}^{n} a_i \varphi_i\left(\tfrac{L}{2}\right)$$

The strain energy due to bending is given by

$$se_b = \frac{1}{2} EI \sum_{i=1,2} \int_0^L \left(\frac{d^2 h_i}{dx^2} - \frac{d^2 w_i}{dx^2} \right)^2 dx \tag{6.3}$$

By normalizing, we get

$$SE_b = \frac{se_b L^3}{E\,I\,h_{mid}^2} = \frac{1}{2}\sum_{i=1,2}\int_0^1 \left(\frac{d^2H_i}{dX^2} - \frac{d^2W_i}{dX^2}\right)^2 dX \tag{6.4}$$

where I is the second moment of the area of cross-section. The axial compression energy of the arches is given by

$$se_c = \frac{1}{4}\frac{EA}{L}\sum_{i=1,2}\left\{\int_0^L \left[\left(\frac{dh_i}{dx}\right)^2 - \left(\frac{dw_i}{dx}\right)^2\right] dx\right\}^2 \tag{6.5}$$

where A is the cross-sectional area of the arches. It is also noted that the arches are assumed to be shallow (i.e., $\left(\frac{dh}{dx}\right)^2 \ll 1$ and $\left(\frac{dw}{dx}\right)^2 \ll 1$), and the curvature and the arc-length of the arch are approximated accordingly to obtain these energy equations. By normalizing the compression energy, we get

$$SE_c = \frac{se_c\,L^3}{E\,I\,h_{mid}^2} = 6Q^2\sum_{i=1,2}\left\{\int_0^L \left[\left(\frac{dH_i}{dX}\right)^2 - \left(\frac{dW_i}{dX}\right)^2\right] dX\right\}^2 \tag{6.6}$$

where $Q = \frac{h_{mid}}{d}$ is a geometric parameter. The work potential due to the applied transverse force f at the mid-span length of $Arch_1$ is given by

$$wp = -f\left(h_1\left(\tfrac{L}{2}\right) - w_1\left(\tfrac{L}{2}\right)\right) \tag{6.7}$$

Normalizing the work potential results

$$\begin{aligned} &WP = -F\delta \\ &F = \tfrac{f\,L^3}{E\,I\,h_{mid}} \quad H_{mid_1} = \tfrac{h_1\left(\frac{L}{2}\right)}{h_{mid}} \quad W_{mid_1} = \tfrac{w_1\left(\frac{L}{2}\right)}{h_{mid}} \\ &\delta = \left(H_{mid_1} - W_{mid_1}\right) \end{aligned} \tag{6.8}$$

The normalized potential energy, PE, is given by

$$\begin{aligned} PE &= SE_b + SE_c + WP \\ &= \frac{1}{2}\sum_{i=1,2}\int_0^1 \left(\frac{d^2H_i}{dX^2} - \frac{d^2W_i}{dX^2}\right)^2 dX + \\ &\quad 6Q^2\sum_{i=1,2}\left\{\int_0^1 \left[\tfrac{1}{2}\left(\tfrac{dH_i}{dX}\right)^2 - \tfrac{1}{2}\left(\tfrac{dW_i}{dX}\right)^2\right] dX\right\}^2 - F\left(H_{mid_1} - W_{mid_1}\right) \end{aligned} \tag{6.9}$$

By substituting Eq. (6.2) in Eq. (6.9), we get the normalized potential energy as

$$\begin{aligned} PE = {} & \frac{1}{4}\left(\sum_{i=1}^{n} a_i^2 M_i^4 + \sum_{i=1}^{n} A_i^2 M_i^4 - 2\sum_{i=1}^{n} a_i A_i M_i^4\right) + \\ & \frac{1}{4}\left(\sum_{i=1}^{n} b_i^2 M_i^4 + \sum_{i=1}^{n} B_i^2 M_i^4 - 2\sum_{i=1}^{n} b_i B_i M_i^4\right) + \\ & \frac{3}{8}Q^2\left(\sum_{i=1}^{n} a_i^2 M_i^2 - \sum_{i=1}^{n} A_i^2 M_i^2\right)^2 + \frac{3}{8}Q^2\left(\sum_{i=1}^{n} b_i^2 M_i^2 - \sum_{i=1}^{n} B_i^2 M_i^2\right)^2 - \\ & F\left(\sum_{i=1,3,5,\cdots}^{n} a_i - \sum_{i=1,3,5,\cdots}^{n} (-1)^{\frac{i+1}{2}} A_i\right) \end{aligned} \tag{6.10}$$

Along with the potential energy of the arches, we must introduce the compatibility condition or the constraint at the common pin joint of the connected arch configuration to obtain the governing equations. Due to the interconnection of the arches through the common revolute joint, the deformation of $Arch_1$ causes the deformation of $Arch_2$ even though $Arch_2$ does not experience any external loading and vice versa. As the revolute joint does not resist the rotation of the arch, the deformed shape of both arches maintains slope continuity at this point. In other words, both $Arch_1$ and $Arch_2$ have the same angle of rotation at the common revolute joint with respect to their as-fabricated states when force is applied to $Arch_1$. Therefore, we impose a rotational compatibility condition at the interconnected revolute joint, which is expressed as:

$$\frac{\left(\left.\frac{dw_1}{dx}\right|_L\right) - \left(\left.\frac{dw_2}{dx}\right|_0\right)}{1 + \left(\left.\frac{dw_1}{dx}\right|_L\right)\left(\left.\frac{dw_2}{dx}\right|_0\right)} = \frac{\left(\left.\frac{dh_1}{dx}\right|_L\right) - \left(\left.\frac{dh_2}{dx}\right|_0\right)}{1 + \left(\left.\frac{dh_1}{dx}\right|_L\right)\left(\left.\frac{dh_2}{dx}\right|_0\right)} \tag{6.11}$$

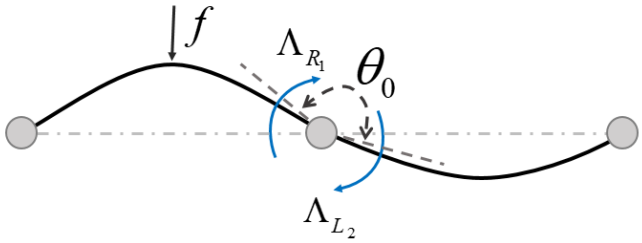

Figure 6.3: A connected arch with the reaction moment and the initial angle difference of the as-fabricated shape at the revolute joint.

In other words, the deformed shape of $Arch_1$ and $Arch_2$ always maintain a constant angle θ_0 at the common pin joint, as shown in Fig. 6.3. As we are considering only shallow arches for the analysis, we neglect the product of slopes in Eq. (6.11), and the revised and normalized constraint equation is given by

$$\left(\frac{dW_1}{dX}\bigg|_L\right)-\left(\frac{dW_2}{dX}\bigg|_0\right)=\left(\frac{dH_1}{dX}\bigg|_L\right)-\left(\frac{dH_2}{dX}\bigg|_0\right) \tag{6.12}$$

The constraint condition at the common revolute joint eventually leads to concentrated complementary moments, Λ_{R_1}, on the right end of $Arch_1$ and Λ_{L_2}, on the left end of $Arch_2$. As the net moment at a revolute joint is always zero, the moments at the common pin joint are equal in magnitude but opposite in nature, i.e.,

$$\Lambda_{R_1} = -\Lambda_{L_2} = \Lambda \tag{6.13}$$

where Λ is the magnitude of the normalized moment at the common pin joint. We obtain the governing equations of the connected arches by minimizing the potential energy with respect to all the deformed mode weights such that the constraint equation given in Eq. (6.13) satisfies, i.e.,

$$\underset{\substack{A_1,A_2,A_3,\cdots \\ B_1,B_2,B_3,\cdots}}{\text{Min}} \quad PE = \frac{1}{2}\sum_{i=1,2}\int_0^1 \left(\frac{d^2H_i}{dX^2} - \frac{d^2W_i}{dX^2}\right)^2 dX +$$

$$6Q^2 \sum_{i=1,2}\left\{\int_0^1 \left[\tfrac{1}{2}\left(\tfrac{dH_i}{dX}\right)^2 - \tfrac{1}{2}\left(\tfrac{dW_i}{dX}\right)^2\right] dX\right\}^2 - F\left(H_{mid_1} - W_{mid_1}\right) \quad (6.14)$$

Subject to:

$$\left(\left.\tfrac{dW_1}{dX}\right|_L\right) - \left(\left.\tfrac{dW_2}{dX}\right|_0\right) - \left(\left.\tfrac{dH_1}{dX}\right|_L\right) + \left(\left.\tfrac{dH_2}{dX}\right|_0\right) = 0$$

The governing equations for the connected arches are obtained from the necessary conditions of the above minimization problem and are expressed as:

$$\frac{M_i^4}{2}\left(A_i - a_i\right) - \frac{3}{2}Q^2C_1\left(A_iM_i^2\right) + F\left\{-(-1)^{\frac{i+1}{2}}\right\}\Big|_{i=1,3,5,\ldots} + \Lambda\left[(-1)^i M_i\right] = 0 \quad (6.15)$$

where $i = 1, 2, 3, \cdots, n$

$$\frac{M_i^4}{2}\left(B_i - b_i\right) - \frac{3}{2}Q^2C_2\left(B_iM_i^2\right) + \Lambda\left[-M_i\right] = 0 \quad (6.16)$$

where $i = 1, 2, 3, \cdots, n$

$$\left\{\sum_1^n A_iM_i(-1)^i\right\} - \left\{\sum_1^n B_iM_i\right\} = \left\{\sum_1^n a_iM_i(-1)^i\right\} - \left\{\sum_1^n b_iM_i\right\} \quad (6.17)$$

where $M_i = i\pi$, $Q = \frac{h_{mid}}{d}$, $C_1 = \sum a_i^2M_i^2 - \sum A_i^2M_i^2$, is the normalized change of arc-length of $Arch_1$, $C_2 = \sum b_i^2M_i^2 - \sum B_i^2M_i^2$, is the normalized change of arc-length of $Arch_2$, and Λ, is the normalized moment acting on both arches. To understand the nature of the force (f) vs. mid-displacement (δ) characteristic of the connected arch, we numerically solve the preceding set of equations given in Eqs. (6.15 – 6.17) and trace the curve for a range of displacement values for both loading and unloading cycles.

As an illustrative example, we take the as-fabricated shapes of both the arches where they consist of only the first mode weight such that, $a_1 = 1$, and $b_1 = 0.5$. We take $h_{mid} =$ 10 mm, $d = 1$ mm, $b = 4$ mm, $L = 100$ mm, $E = 50$ MPa for both the arches. Using Eq. (6.15), we solve for f by varying δ from 0 mm to twice the height of the arch, i.e., 20 mm, to get the $f - \delta$ curve for the loading cycle. Similarly, to get the $f - \delta$ curve for the

unloading cycle, we vary δ in a reverse way. The force-displacement and mode weights-displacement characteristics of these connected arches are shown in Fig. 6.4.

The connected arch we are considering for the example has two stable state configurations. In Fig. 6.4a-d, O represents the as-fabricated shape of $Arch_1$ where the mid-point has a zero displacement, and E represents the second force-free state of the connected arches. The arch follows the path $OABCDEF$ (blue-solid curve) for the loading cycle and $FECGAO$ (magenta-solid curve) for the unloading cycle. The initial phase $O-A$ and the post-buckling phase $E-F$ are identical for both the loading and unloading cycle, whereas, for a displacement value between A and E, there are two different arch configurations and force values exist for the loading and unloading cycle, leading to two different force-displacement pathways. These two pathways lead to two different strain energy landscapes for the loading and unloading phases. During the loading cycle, at point A, the energy that corresponds to the path $ABCDE$ is lower than the energy that corresponds to the path $AGCE$. Therefore, the arches follow the lower energy path, $ABCDE$ while loading. A similar argument can be drawn for the unloading path also.

As we apply load or displacement to $Arch_1$, the slope at both ends starts increasing. But due to the rotational stiffness of $Arch_2$, the slope at the right end of $Arch_1$ gets restricted when compared to its left end. The arches act as nonlinear rotational springs to each other, which leads to asymmetry in the system. Therefore, the arches deform asymmetrically due to the coupling at the common revolute joint, which produces an extra torque at one end of these arches, despite of symmetric loading and boundary conditions. Hence with a change in displacement value, the magnitude of the first mode weights starts decreasing, and that of the second and third modes start increasing for both the arches (see Fig. 6.4c-d). With a further increment of displacement, the force value increases till it reaches the switching force and decreases smoothly (curve $O-A-B$) till it reaches point B. At point B, the force and the stiffness suddenly jump to a lower value. This sudden jump occurs as the net rotation of $Arch_2$ at the common revolute joint reaches a threshold value (see Fig. 6.4b) and switches to its inverted shape (see Fig. 6.4d-e). As shown in Fig. 6.4c, the second mode weight of $Arch_1$ attains a maximum at this point and starts decreasing gradually till point D. At this point D, the second mode weight for $Arch_1$ suddenly jumps to point E by choosing the least strain energy path and becomes negative (see Fig. 6.4c). The change in the second mode

weight helps the arch to release additional axial thrust by suddenly changing its configuration, as shown in Fig. 6.4e. The same argument can also be made for the unloading path $FECGAO$ when we vary the displacement in a reverse direction starting from the point F. We decide the nature of the connected arches based on their switching nature and stability at the inverted shape.

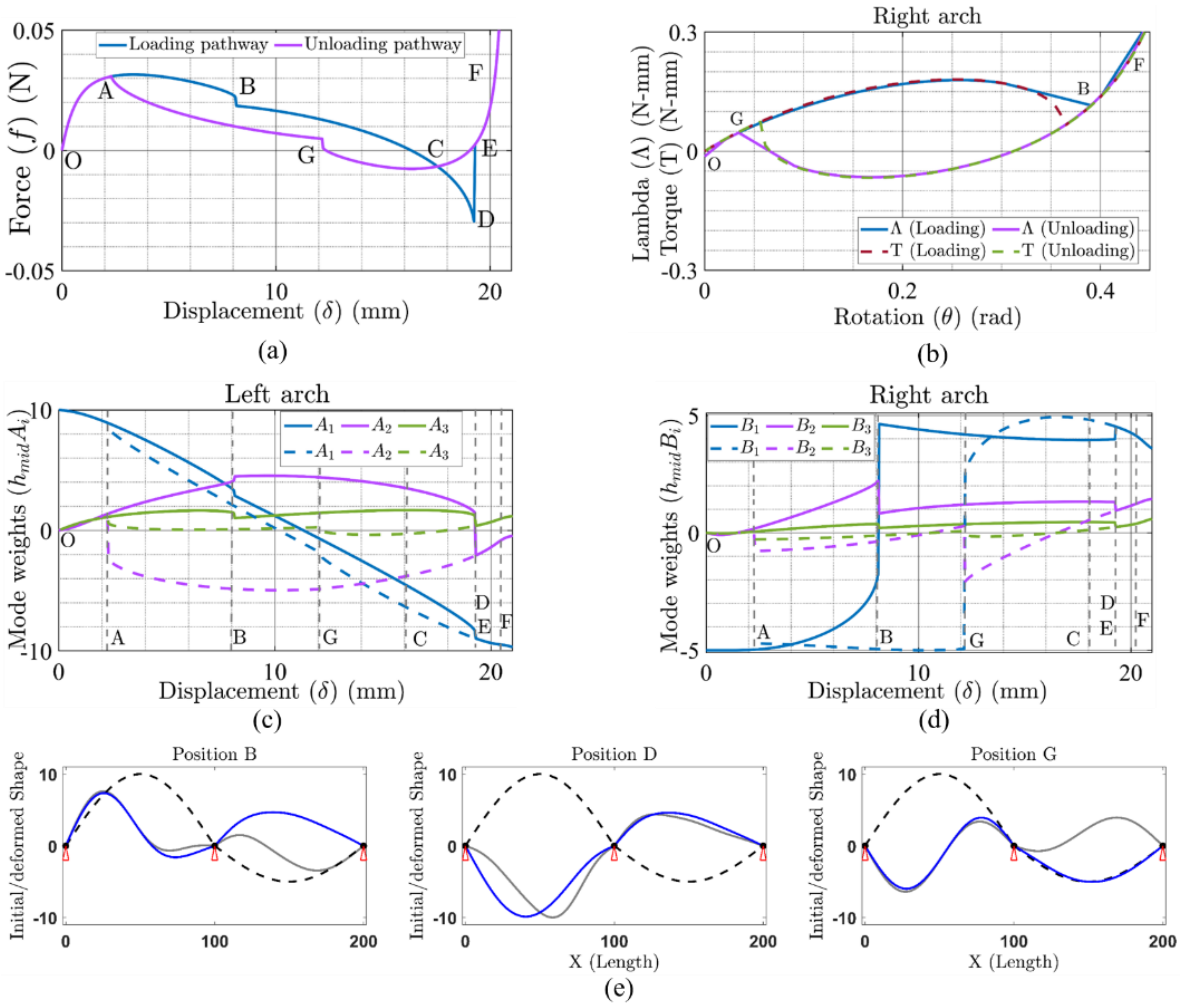

Figure 6.4: (a) Force-displacement ($f-\delta$) characteristics of the connected arch showing the loading path and the unloading path, (b) comparison loading and unloading pathways of torque (T)-rotation (θ) characteristics (solid curve) with the multiplier (Λ)-rotation (θ) characteristics (dashed curve) for $Arch_2$. Note that a concentrated torque (T) is applied at the left end of $Arch_2$, (c) mode weights variations of $Arch_1$ w.r.t the displacement, (d) mode weights variations of $Arch_2$ w.r.t the displacement, and (e) the as-fabricated and deformed state of the arches at positions B, D, and G. In (c) and (d), the solid line corresponds to the loading path, and the dotted line represents the unloading path. In (e), the grey-dashed line shows the as fabricated shape, the grey-solid line shows the deformed shape just before the position B, D, and G, and the blue-solid line shows the deformed shape of the arches at positions B, D, and G.

6.3 Calculating switching and switchback loads

The switching point corresponds to the maximum force with respect to the displacement on the force-displacement curve, whereas the switchback point corresponds to the minimum force value. To get these switching points of the arch, we pose an optimization problem as follows.

$$\underset{\substack{A_1,A_2,A_3,\cdots \\ B_1,B_2,B_3,\cdots}}{\text{Min or Max}}: \quad F$$

subject to:

$$\frac{M_i^4}{2}\left(A_i - a_i\right) - \frac{3}{2}Q^2C_1\left(A_iM_i^2\right) + F\left\{-(-1)^{\frac{i+1}{2}}\right\}\Big|_{i=1,3,5,\ldots} + \Lambda\left[(-1)^i M_i\right] = 0 \quad (6.18)$$

$$\frac{M_i^4}{2}\left(B_i - b_i\right) - \frac{3}{2}Q^2C_2\left(B_iM_i^2\right) + \Lambda\left[-M_i\right] = 0$$

$$\left\{\sum_1^n A_iM_i(-1)^i\right\} - \left\{\sum_1^n B_iM_i\right\} = \left\{\sum_1^n a_iM_i(-1)^i\right\} - \left\{\sum_1^n b_iM_i\right\}$$

We numerically solve the preceding optimization problem to get the switching, switchback force, and their corresponding unknown mode weights, A_is and B_is so that they satisfy the equilibrium equations, which are nothing but the KKT (Karush-Kuhn-Tucker) necessary conditions for the constrained optimization problem. The problem becomes easier when we consider only a few mode shapes to represent the shape of the arches. From our earlier studies, we found that the first three mode shapes are adequate to get accurate results.

For the particular arch considered here, the switching and switchback forces are 0.0315 N and 0.0075 N, respectively. We also found that $Arch_2$ switches to an inverted shape when $Arch_1$ switches, which is desirable to obtain a flip-flop mechanism.

6.4 Finding second stable state configuration

The second stable state of the connected arch corresponds to a zero-force configuration other than the as-fabricated shape. Also, it represents a minimum on the strain energy landscape. To get the bistable configuration of the connected arches, we solve Eqs. (6.15 – 6.17) by substituting $F = 0$. Once we get a solution, we check for the sufficiency condition to confirm the solution has minimum energy. Hence, we calculate the determinant of the principal minors of the bordered hessian matrix, $\mathbf{H_b}$, which is expressed as

$$\mathbf{H_b} = \begin{bmatrix} [0]_{1\times1} & [\Theta_1]_{1\times n} & [\Theta_2]_{1\times n} \\ [\Theta_1{}^{\mathrm{T}}]_{n\times1} & [\mathbf{H}_1]_{n\times n} & [0]_{n\times n} \\ [\Theta_2{}^{\mathrm{T}}]_{n\times1} & [0]_{n\times n} & [\mathbf{H}_2]_{n\times n} \end{bmatrix}_{(1+2n)\times(1+2n)} \tag{6.19}$$

where n is the number of mode weights taken to approximate the shape of the arches and the vector Θ_1, Θ_2 and the matrix $\boldsymbol{H_1}$, $\boldsymbol{H_2}$ are obtained by

$$\begin{aligned} \Theta_1 &= (-1)^i\, i\pi \\ \Theta_2 &= -i\pi \\ (\mathbf{H}_1)_{ii} &= \frac{M_i^4}{2} - \frac{3Q^2 M_i^2 C_1}{2} + 3Q^2 A_i^2 M_i^4 \\ (\mathbf{H}_1)_{ij} &= 3Q^2 A_i A_j M_i^2 M_j^2 \\ (\mathbf{H}_2)_{ii} &= \frac{M_i^4}{2} - \frac{3Q^2 M_i^2 C_2}{2} + 3Q^2 B_i^2 M_i^4 \\ (\mathbf{H}_2)_{ij} &= 3Q^2 B_i B_j M_i^2 M_j^2 \end{aligned} \tag{6.20}$$

A stable configuration is confirmed if the determinants of the last $2n-1$ principal minors of the bordered hessian matrix (Eq. 6.19) become negative. The bistability of a connected arch configuration is determined by the shape of the individual arch shape. For certain configurations, the inverted states may not show any bistability even though they are bistable individually when they are not connected to each other. The switching and bistability criteria of the connected arches will be discussed in detail in Section 6.4.

6.5 Validation using finite element analysis

we validate our mathematical model with the results obtained from finite element analysis (FEA) for different kinds of as-fabricated arch configurations and found a good agreement (within 3% error at the switching and switchback point) between them, as shown in Fig. 6.5. The solid curve represents the results obtained from the semi-analytical modeling considering first five mode shapes ($n = 5$) to approximate the deformed shape, and the dashed curve is obtained from FEA. The blue and the magenta curves represent the loading and unloading paths, respectively. We have taken $h_{mid} = 10$ mm, $d = 1$ mm, $b = 4$ mm, $L = 100$ mm, and $E = 50$ MPa for all the examples. The FEA was performed in ABAQUS using continuum 2D quadrilateral elements, and the curve was obtained from the quasi-static

dynamic-implicit analysis with geometric nonlinearities for all the cases. Like the analytical modeling, FEA also shows different pathways for the loading and unloading cycle. Both analyses show a kink at the switching and switchback point due to sudden asymmetric mode switching. However, the semi-analytical model we propose is more computationally effective than the FEA. The semi-analytical method solves the problem within a CPU time of 20 seconds compared to 700 seconds of FEA, and thus, it is 35 times faster. The computation time in FEA may vary from problem to problem, and it may take longer time if we go for a 3D analysis. Nevertheless, a mathematical model always solves the problem much faster than the FEA and is useful in designing the connected arches for different functionality.

In the first two examples (Fig. 6.5a-b), the as-fabricated shapes of $Arch_1$ and $Arch_2$ consist of only the first mode shape in their as-fabricated shape. In the first case (Fig. 6.5a), both the arches have equal magnitude, whereas in the second case, they are of different magnitudes. In the first case, although $Arch_1$ switches to its inverted shape, $Arch_2$ does not switch. They also do not show bistability, even though these arches show bistability individually. However, in the second case, we keep the as-fabricated shape of $Arch_1$ same as the first case and reduce the magnitude of $Arch_2$ height to half of the $Arch_1$ height. In this case, the arches not only switch to their inverted shapes but also show bistability. In the third example (Fig. 6.5c), we take an asymmetric $Arch_1$ shape that does not have a second stable state configuration. We connect the $Arch_1$ with a symmetric and bistable $Arch_2$ shape. When these two arches are connected to each other, both the arches change their curvature, but they return to their original undeformed state as soon as we remove the load.

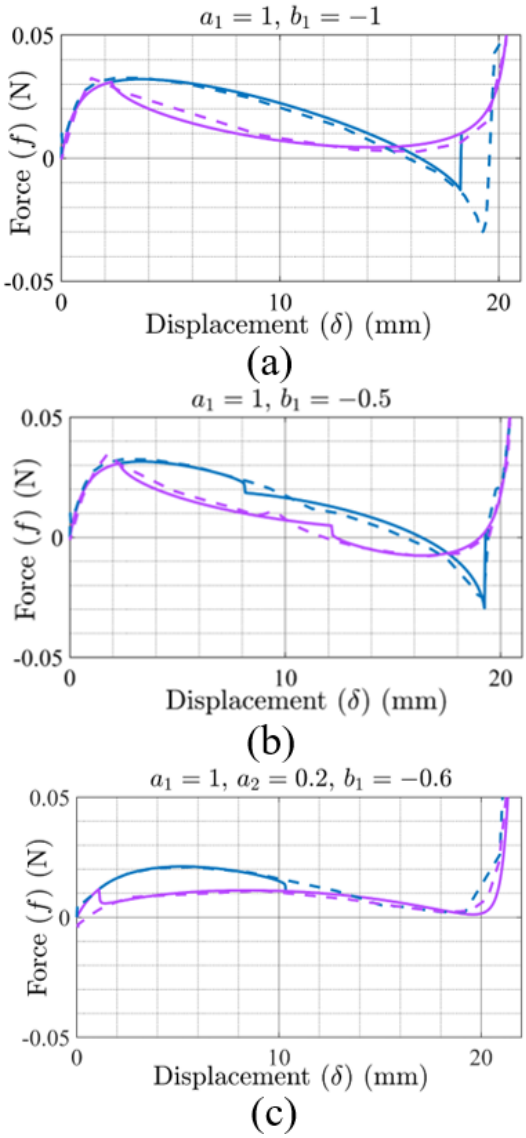

Figure 6.5: Comparison of force-displacement characteristics with FEA for different as-fabricated shapes. (a) $Arch_2$ does not switch to its inverted shape, and the configuration does not show bistability, (b) $Arch_2$ switches to its inverted shape, and the configuration shows bistability, and (c) $Arch_2$ switches to its inverted shape, but the configuration does not show bistability. The solid lines are the results from analytical modelling, and the dashed lines are for FEA. The blue and magenta lines represent the loading and unloading paths, respectively.

Based on $Arch_2$ deformation and the stability of the combined configuration, the nature of the connected arches can fall into four different categories, like, (i) *switching and bistable (SB)*, (ii) *switching but not bistable (SNB)*, (iii) *not switching and not bistable (NSNB)*, (iv) *not switching but bistable (NSB)*. Here, the switching refers to the flipping of $Arch_2$ to its inverted shape, i.e., the curvature of $Arch_2$ changes its sign due to the moment caused by the deformation of $Arch_1$. These connected arches are called bistable if these

structures have a second force-free state other than their initial as-fabricated shape; otherwise, they are not bistable. The nature of these connected arches depends on the geometry of the individual arch and the external force or displacement that applied to $Arch_1$. These connected arches have various unique applications like logic gates, therapeutic footwear, and several others. Hence, in this chapter, we seek to understand the nature of any two random-shaped arch when they are connected to each other: (1) will $Arch_2$ flip or switch to its inverted shape for a given mid-point displacement of $Arch_1$? (2) If $Arch_2$ flip to its inverted shape, will the combined arch configuration show bistability? These questions will be answered in this section with the help of the torque (Λ) vs. rotation (θ) diagram of the individual arch.

6.6 Condition for flipping

To understand the switching conditions of the connected arches, we need to study the governing equations of the individual arches and their constraint equation separately. At first, let us consider the governing equation of $Arch_2$, as expressed in Eq. (6.16). We can observe that, $Arch_2$ experience an end moment at the left end of the arch due to the rotation of $Arch_1$. Initially, both the arches are in their undeformed state, and there is no moment at the common pin joint. As $Arch_1$ starts deforming, moment, Λ, at the common pin joint and the end rotation, θ, of $Arch_2$ also starts increasing from point O, as shown in Fig 6.6a. Finally, when the rotation of the arch exceeds a critical angle (point B, as shown in Fig. 6.6a), $Arch_2$ suddenly switches from point A to point B by toggling its shape, as shown in Fig. 6.6b. It is noted that we obtain the switching or critical point of $Arch_2$ by solving

$$\frac{d\,\theta}{d\,C_2} = 0 \tag{6.21}$$

where C_2 is the normalized arc-length of $Arch_2$. To get the expression of θ in terms of C_2, we first express the end moment, Λ, as

$$\left(\sum \frac{1}{\frac{1}{4}\left(M_i^2 - 3Q^2C_2\right)^2}\right)\Lambda^2 - \left(\sum \frac{b_i M_i^3}{\frac{1}{4}\left(M_i^2 - 3Q^2C_2\right)^2}\right)\Lambda + \left(\sum \frac{b_i^2 M_i^6}{\left(M_i^2 - 3Q^2C_2\right)^2} - \sum b_i^2 M_i^2 + C_2\right) = 0 \tag{6.22}$$

In Eq. (6.22), we get two moment values (Λ) for both the switching and the switchback path for a range of arc-length values (C_2). Once we get Λ from Eq. (6.22), we get the end rotation as

$$\theta = \sum b_i M_i - \sum \frac{\left(\frac{1}{2} b_i M_i^3\right) - \Lambda}{\frac{1}{2}\left(M_i^2 - 3Q^2 C_2\right)} \tag{6.23}$$

Using Eq. (6.23), we can get a set of rotation values, θ, for a range of C_2 value, and can obtain the critical or the switching point, (Λ_c, θ_c), using Eq. (6.21).

Now, let us consider the governing equation of $Arch_1$ as expressed in Eq. (6.15). We can observe that, $Arch_1$ experience loading at the mid-point and a moment at the right support. We assume the load in terms of displacement and establish a switching condition for a specified mid-displacement of $Arch_1$. As shown in Fig. 6.7, δ is the maximum mid-point displacement we are providing to $Arch_1$, and for this displacement, we check if $Arch_2$ switches to its inverted shape.

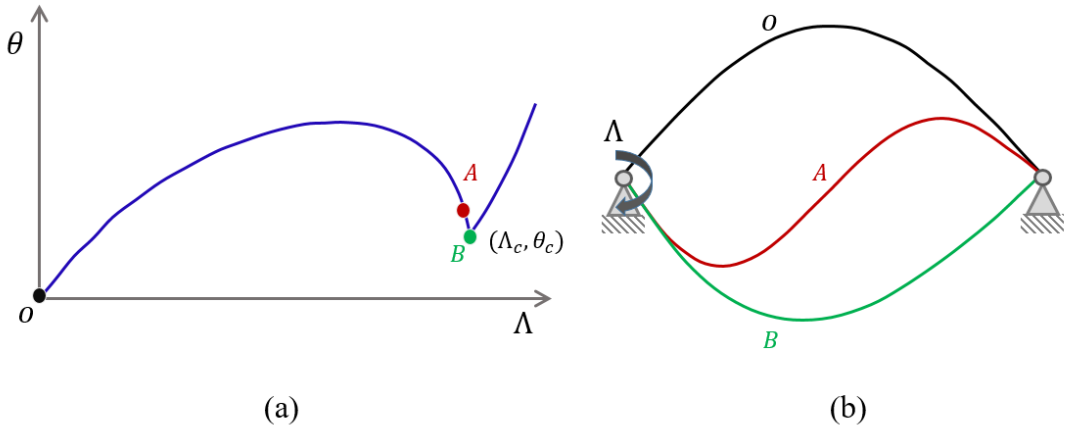

Figure 6.6: (a) $\Lambda - \theta$ characteristic curve of $Arch_2$ when an end moment acts at the left end of the arch. O be the initial as-fabricated state, A is the state before switching to the toggle state B. The state at B is represented by (Λ_c, θ_c), (b) the initial state and the deformed states of the arch.

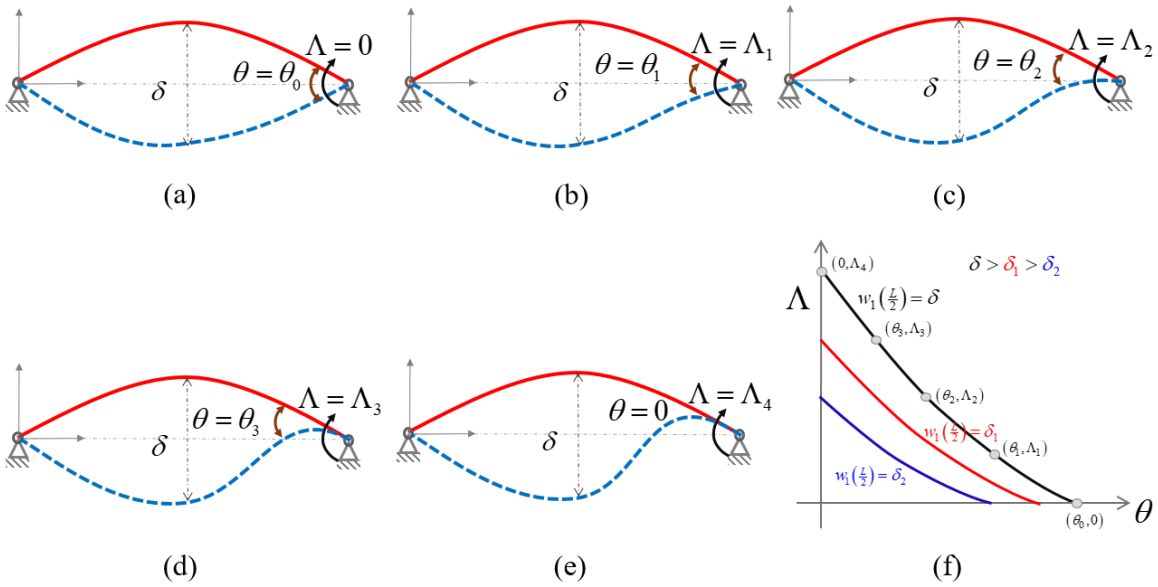

Figure 6.7: (a-e) Schematics showing the change of angular rotations between the initial and the deformed shape of $Arch_1$ for different end torque values keeping a constant mid-displacement value as δ, (b) $\Lambda - \theta$ characteristic curve of $Arch_1$ for various mid-displacement values.

Along with the displacement, $Arch_1$ also experience a moment at the right pin joint. This moment arises due to the presence of $Arch_2$, and its magnitude depends on the equivalent rotational stiffness of $Arch_2$. Assuming there is no $Arch_2$, implies there is no opposing moment acting due to the torsional spring at the right end of $Arch_1$, then the end rotation of $Arch_1$ would be θ_0 for a displacement of δ at the center, as shown in Fig. 6.7a. As we add different shapes of $Arch_2$, i.e., if the equivalent rotational stiffness of arches increases, the end rotation of $Arch_1$ gradually decreases to zero, and the slope of the deformed and the initial profile of $Arch_1$ coincides with each other, as shown in Fig. 6.7b – e. The relation of angular rotation, θ, and the end moment, Λ, for various mid-displacement of $Arch_1$ is shown in Fig. 6.7f. The implicit mathematical expression that describes the relation between Λ and θ of $Arch_1$ for a specified mid-displacement, δ, is expressed as

$$\frac{3}{2}Q^2\left[\sum a_i^2 M_i^2 - A_1^2 M_1^2 - \left(\theta + A_1 M_4 + \delta h_{mid} M_3\right)^2 - \left(A_1 + \delta h_{mid}\right)^2 M_3^2\right]\left[\left(\theta + A_1 M_4 + \delta h_{mid} M_3\right) M_2\right] \qquad (6.24)$$
$$-\frac{1}{2}\left[\left(\theta + A_1 M_4 + \delta h_{mid} M_3\right) M_2^3 - a_2 M_2^4\right] - \Lambda M_2 = 0$$

where the expression of the first mode weight, A_1, is given by

$$A_1 = \frac{-1}{3R_3}\left(R_2 + \bar{\mathbb{C}} + \frac{\Delta_0}{\bar{\mathbb{C}}}\right) \tag{6.25}$$

and the expression for $\bar{\mathbb{C}}$, Δ_0, R_2, and R_3 are given as

$$\begin{aligned}
R_3 &= 390Q^2\pi^4 \\
R_2 &= 981\delta h_{mid}Q^2\pi^4 + 120Q^2\pi^3\theta \\
R_1 &= -15C_0Q^2\pi^2 + 41\pi^4 + 837\delta^2h_{mid}^2Q^2\pi^4 + 198\delta h_{mid}Q^2\pi^3\theta + 15Q^2\pi^2\theta^2 \\
R_0 &= -0.5a_1\pi^4 - 40.5a_3\pi^4 + 40.5\delta h_{mid}\pi^4 - 13.5C_0\delta h_{mid}Q^2\pi^2 + 243\delta^3h_{mid}^3Q^2\pi^4 \\
&\quad - 4\pi\Lambda + 81\delta^2h_{mid}^2Q^2\pi^3\theta + 13.5\delta\, h_{mid}Q^2\pi^2\theta^2 \\
\Delta_0 &= R_2^2 - 3R_3R_1 \\
\Delta_1 &= 2R_2^3 - 9R_1R_2R_3 + 27R_3^2R_0 \\
\mathbb{Q} &= \sqrt{\Delta_1^2 - 4\Delta_0^3} \\
\bar{\mathbb{C}} &= \sqrt[3]{\tfrac{1}{2}\left(\mathbb{Q} + \Delta_1\right)}
\end{aligned} \tag{6.26}$$

To get the equilibrium configuration of the connected arches for different δ values, we finally consider the constraint equation (Eq. 6.17). According to the constraint equation, the moment, Λ, and the rotation, θ, must be equal for both arches at any instant. It implies the intersection of $\Lambda - \theta$ characteristics plot (Fig. 6.6a and Fig. 6.7f) of both the arches will give us the equilibrium configuration (marked as a black-solid circle), as shown in Fig. 6.8. For a specified mid-displacement, δ, if the rotation value at the equilibrium configuration is more than the critical rotation value of $Arch_2$, we can say that $Arch_2$ has flipped to its inverted shape. Hence to check if $Arch_2$ flips to its inverted shape, we check the position of the switching point $((\theta_c, \Lambda_c))$ of $Arch_2$. When the switching point falls inside or on the $\Lambda - \theta$ characteristic curve of $Arch_1$, we confirm that $Arch_2$ flips to its inverted state; otherwise $Arch_2$ does not flip. Hence the switching condition of $Arch_2$ can be expressed by relacing θ and Λ with θ_c and Λ_c, respectively in Eq. (6.25) and then by checking its sign. In other words, to ensure the flipping of $Arch_2$, Eq. (6.24) must result in a negative value for a θ_c and Λ_c value of $Arch_2$, i.e.,

$$\begin{aligned}
&\frac{3}{2}Q^2\left[\sum a_i^2M_i^2 - A_1^2M_1^2 - \left(\theta + A_1M_4 + \delta h_{mid}M_3\right)^2 - \left(A_1 + \delta h_{mid}\right)^2M_3^2\right]\left[\left(\theta + A_1M_4 + \delta h_{mid}M_3\right)M_2\right] \\
&-\frac{1}{2}\left[\left(\theta + A_1M_4 + \delta h_{mid}M_3\right)M_2^3 - a_2M_2^4\right] - \Lambda M_2\Big|_{(\theta_c,\Lambda_c)} \le 0
\end{aligned} \tag{6.27}$$

Eq. (6.27) must satisfy to get a flip-flop mechanism. It is noted that we obtain θ_c and Λ_c value for $Arch_2$ using Eqs. (6.21 – 6.23).

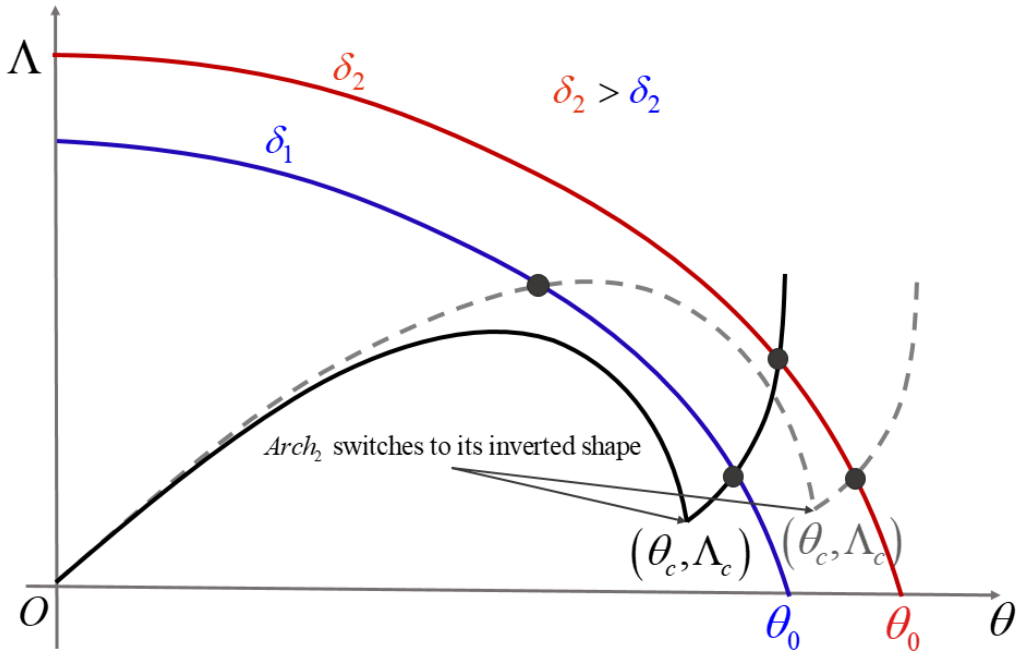

Figure 6.8: Schematics of $\Lambda - \theta$ characteristic curve of both the arches for two different $Arch_2$ shapes (the solid-black curve and the gray-dash curve), and for two different mid-displacement (δ_1 and δ_2) of $Arch_1$. The equilibrium configuration is marked as a black-solid circle. As we can see for the mid-displacement δ_1, the arch shape corresponding to the black-solid curve toggles to its inverted shape, but the other arch does not switch. However, for the mid-displacement δ_2, both the arches toggle to their inverted shape.

6.7 Condition for bistability

Once both the arches switch to their inverted shape, we check if a force-free stable state configuration exists. With the removal of the transverse load on $Arch_1$, both the arches only experience an end moment, and the equilibrium equations of the arches change to

$$\frac{M_i^4}{2}\left(A_i - a_i\right) - \frac{3}{2}Q^2 C_1\left(A_i M_i^2\right) + \Lambda\left[(-1)^i M_i\right] = 0 \tag{6.28}$$

$$\frac{M_i^4}{2}\left(B_i - b_i\right) - \frac{3}{2}Q^2 C_2\left(B_i M_i^2\right) + \Lambda\left[-M_i\right] = 0 \tag{6.29}$$

$$\left\{\sum_1^n A_i M_i (-1)^i\right\} - \left\{\sum_1^n B_i M_i\right\} = \left\{\sum_1^n a_i M_i (-1)^i\right\} - \left\{\sum_1^n b_i M_i\right\} \tag{6.30}$$

To know if the connected arches configuration has a second stable state, we need to study the $\Lambda - \theta$ characteristics of both $Arch_1$ and $Arch_2$ separately. We can obtain the $\Lambda - \theta$

characteristics for $Arch_2$ using Eqs. (6.22 – 6.23) for different normalized arc-length of $Arch_2$, C_2. Similarly, the $\Lambda-\theta$ characteristics for $Arch_1$ can be expressed in terms of the normalized arc-length of $Arch_1$, C_1, as:

$$\left(\sum\frac{1}{\frac{1}{4}\left(M_i^2-3Q^2C_1\right)^2}\right)\Lambda^2-\left(\sum\frac{(-1)^i a_i M_i^3}{\frac{1}{4}\left(M_i^2-3Q^2C_1\right)^2}\right)\Lambda+\left(\sum\frac{a_i^2M_i^6}{\left(M_i^2-3Q^2C_1\right)^2}-\sum a_i^2M_i^2+C_1\right)=0 \tag{6.31}$$

$$\theta=\sum(-1)^i a_iM_i-\sum\frac{(-1)^i\left(\frac{1}{2}a_iM_i^3\right)-\Lambda}{\frac{1}{2}\left(M_i^2-3Q^2C_1\right)} \tag{6.32}$$

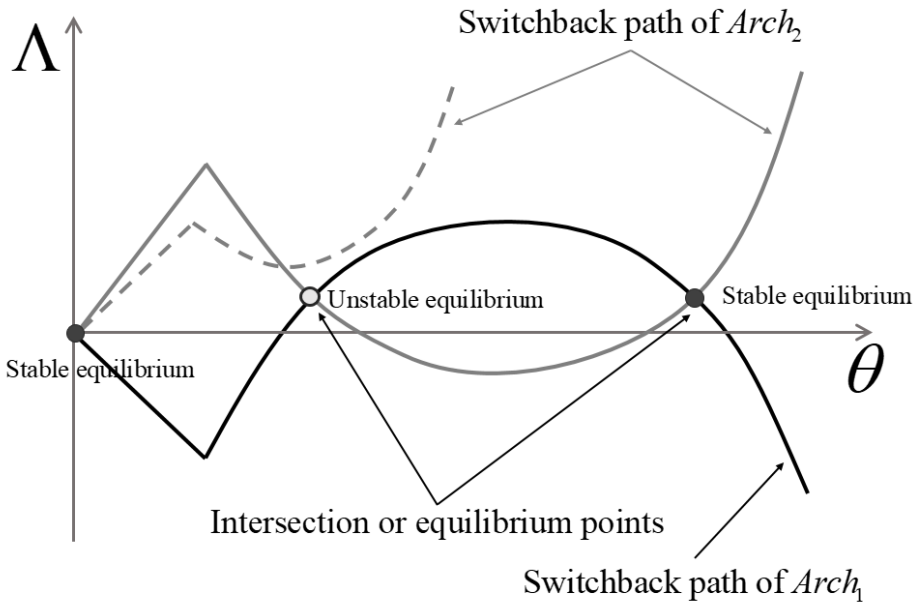

Figure 6.9: Schematics of $\Lambda-\theta$ characteristic curve of switchback path of the arches for two different $Arch_2$ shapes (grey-solid curve and gray-dash curve), and for a particular $Arch_1$ shape. The $Arch_2$ shape corresponding to the grey-dash curve has only one stable state at the initial shape. However, the $Arch_2$ shape corresponding to the grey-solid curve has two stable state configurations. The stable states are represented by a black-solid circle, and the unstable state is represented by a white-solid circle.

Bistability of the connected arch can be obtained by getting the $\Lambda-\theta$ nature of the individual arches and their intersection points. Because of the stored strain energy at the inverted state, these arches try to attain an energy minimum by switching back to their second stable state. Hence, both the arches follow the switchback path of their $\Lambda-\theta$ characteristics curve. As the constraint equation in Eq. (6.30) also must satisfy, these switchback curves of the arches must intersect at their equilibrium configuration. We obtain

the switchback path of $\Lambda - \theta$ characteristics curve for $Arch_1$ by using Eqs. (6.31 – 6.32) and for $Arch_2$ by using Eqs. (6.22 – 6.23), and check if they intersect with each other. If the connected arch configuration does not have a second stable state, the stored energy comes to zero by retaining the initial arch configuration, as shown by O in Fig. 6.9. In case of the existence of another stable state configuration, the connected arch attains a minimum energy state, and the switchback path of both the arches intersect (other than point O), as shown in Fig. 6.9. In case the configuration becomes bistable, there also exists an unstable zero-force state in-between the two stable states. Based on the stability characteristic of the individual arch, we demonstrate four possible conditions to obtain a bistable connected arch configuration, as shown in Fig. 6.10. It is noted that the connected arch will never result in a bistable configuration if the individual arch does not show bistability. Also, to get a flip-flop mechanism, the connected arch configuration must obey the switching and the bistability criteria simultaneously.

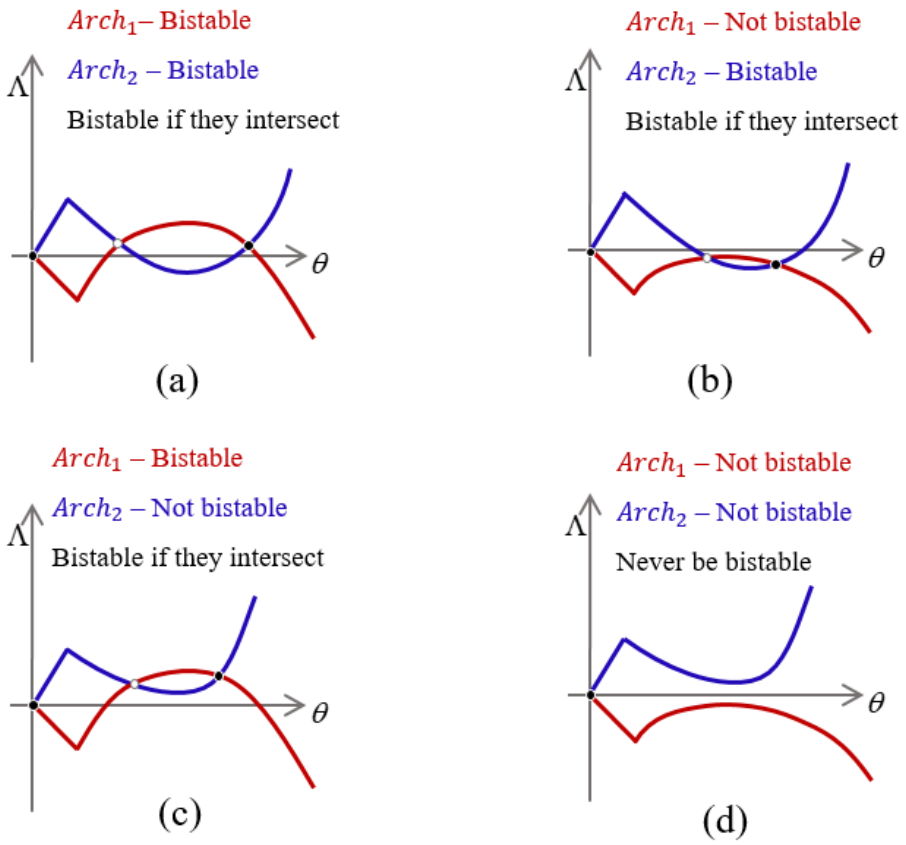

Figure 6.10: Schematics of $\Lambda - \theta$ characteristic curve of switchback path of the arches and their nature for different arch types.

Illustrative examples

To validate our model, we choose three different arch combinations and predict their nature by using the switching and bistability conditions, as shown in Fig. 6.11. The elastic modulus (E) is taken to be 4200 MPa, the length of the individual arch (L) is assumed to be 100 mm, the in-plane width (w) is taken to be 1 mm, the out-of-plane breadth (b) is taken to be 4 mm, and the geometric constant (Q) is assumed to be 10 for all three cases. The maximum mid-displacement of $Arch_1$ is expressed in terms of mid-height (h_{mid}) of $Arch_1$ in the downward direction as $\delta = 2.2 * h_{mid}$. For example, if the mid-span height of $Arch_1$ is 10 mm, the maximum displacement, δ, provided at the center of $Arch_1$ is 22 mm in the downward direction.

In *Example 1*, $Arch_2$ does not switch to its toggle state for the prescribed mid-displacement of $Arch_1$ as the switching point, (θ_c, Λ_c), of $Arch_2$ fall outside the $\Lambda - \theta$ curve (maroon-solid curve) of $Arch_1$. Hence the nature of the connected arch configuration is *NSNB*. However, in *Example 2* and *Example 3*, the critical switching point falls inside the $\Lambda - \theta$ curve of $Arch_1$. Hence, for both the connected arch configurations, $Arch_2$ toggles and changes its curvature. In *Example 2*, the nature of the configuration is *SNB*, as the as-fabricated shape is the only stable state configuration. However, in *Example 3*, the switchback paths of the arches intersect with each other, and the configuration has a second stable state when both the arches are at their inverted shapes. Hence, the nature of this connected arch configuration is *SB*.

Examples	Checking for switching	Checking for bistability	Comments
Example – 1 $h_1(x) = 10\sin\left(\frac{\pi x}{100}\right)$ $h_2(x) = -10\sin\left(\frac{\pi x}{100}\right)$	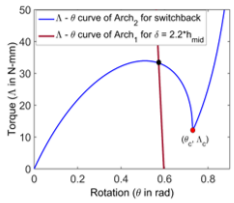		$Arch_2$ does not switch to its inverted shape as the switching point, (θ_c, Λ_c), is outside the $\Lambda - \theta$ curve of $Arch_1$.
Example – 2 $h_1(x) = 10\sin\left(\frac{\pi x}{100}\right) + 2\sin\left(\frac{2\pi x}{100}\right)$ $h_2(x) = -6\sin\left(\frac{\pi x}{100}\right)$	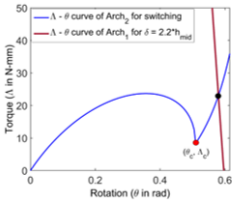	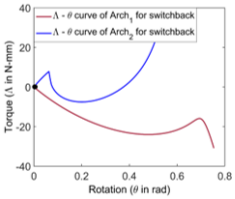	$Arch_2$ switches to its inverted shape as the switching point, (θ_c, Λ_c), is inside the $\Lambda - \theta$ curve of $Arch_1$. However, the configuration is not bistable as the switchback paths do not intersect with each other.
Example – 3 $h_1(x) = 10\sin\left(\frac{\pi x}{100}\right)$ $h_2(x) = -7\sin\left(\frac{\pi x}{100}\right)$	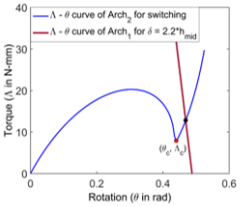	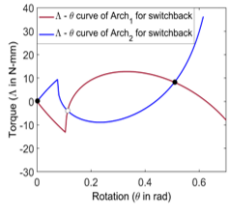	$Arch_2$ switches to its inverted shape as the switching point, (θ_c, Λ_c), is inside the $\Lambda - \theta$ curve of $Arch_1$. Also, the configuration has a second stable state configuration as the switchback paths intersect with each other.

Figure 6.11: Prediction of the nature of connected arch configurations for different $Arch_1$ and $Arch_2$ shapes using the switching and bistability conditions.

6.8 Design domain for different $Arch_1$ shapes

Based on the analysis and design model we discussed in the previous sections, we obtain the design domain by identifying the regions of *SB*, *SNB*, and *NSNB* for various kinds of arch combinations, keeping. We obtain design domains for three different $Arch_1$ shapes and verify our theory using 3D-printed prototypes. The length of the arches is taken to be 100 mm, the in-plane depth is taken to be 1 mm, and the geometric parameter Q is taken as 10 in all the configurations. In all three cases, the as-fabricated shape of $Arch_1$ remains unchanged, whereas the as-fabricated shape of $Arch_2$ is changed to obtain the design domain. The as-fabricated shape of $Arch_1$ is taken to be $10\sin\left(\frac{\pi x}{100}\right)$ in the first example (see Fig. 6.12), $10\sin\left(\frac{\pi x}{100}\right) + 2\sin\left(\frac{3\pi x}{100}\right)$ in the second example (see Fig. 6.14), and $10\sin\left(\frac{\pi x}{100}\right) + 2\sin\left(\frac{2\pi x}{100}\right)$ in the third example (see Fig. 6.16). In all three examples, the as-fabricated shapes of $Arch_2$ is varied such that the first mode weight $b_1 \in [-1, -0.5]$, the second mode weight $b_2 \in [-0.05, -0.5]$, and the third mode weight $b_3 \in [-0.39, 0]$.

The design domain for various $Arch_2$ shapes for the first example is presented in Fig. 6.12. The black color region in Fig. 6.12 indicates the *NSNB* domain, the grey color

region indicates the *SNB* domain, and the white color region indicates the *SB* domain. It is observed that when the magnitude of the third mode weight $b_3 \in [-0.21,0]$ the whole region is divided into two regions – the *SB* and the *NSNB*. As we increase the magnitude of the third mode weight, the critical switching rotation value of $Arch_2$ decreases, and the *NSNB* region slowly converts into the *SB* region for $b_3 < -0.21$. As we further increase b_3 beyond-0.31, $Arch_2$ loses its bistability nature even though they flip to their inverted shape. To check the accuracy of our developed model, we randomly picked three connected arch configurations from each example. We 3D print them and test them to verify their nature with the modelling (see Fig. 6.13, Fig. 6.15, and Fig. 6.17).

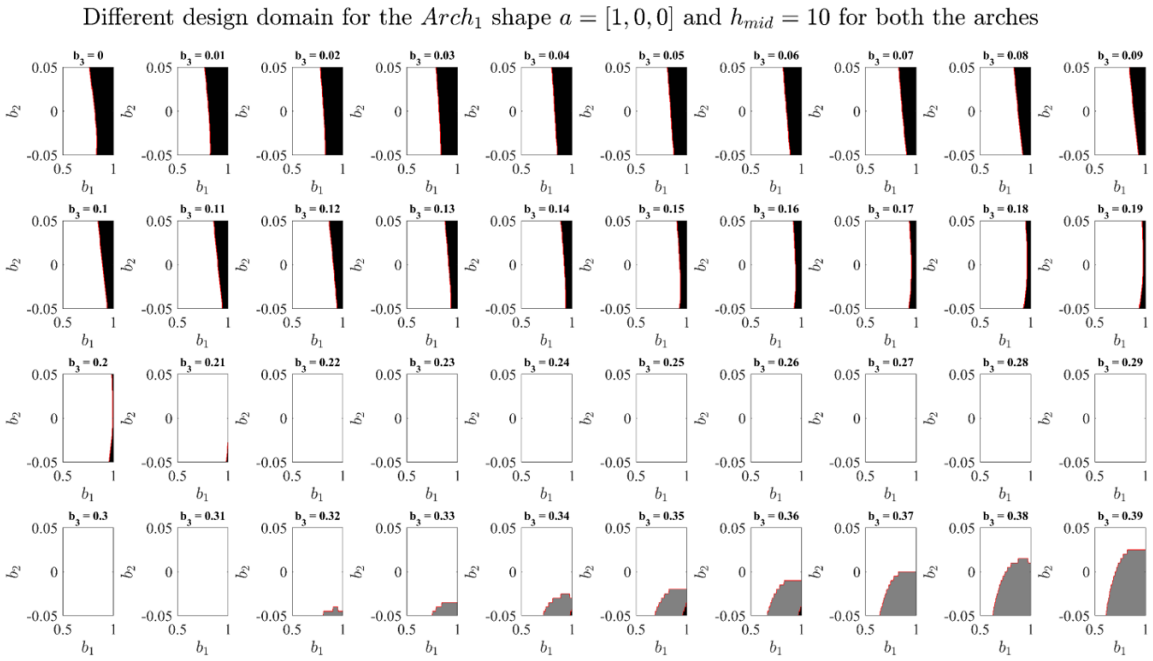

Figure 6.12: Design domain for the $Arch_1$ shape $a = [1, 0, 0]$. The black color region indicates the *not-switching and not-bistable* (NSNB) domain, the grey indicates the s*witching and not-bistable* (SNB) domain, and the white indicates the *switching and bistable* (SB) domain. h_{mid} is taken to be 10 for both the cases.

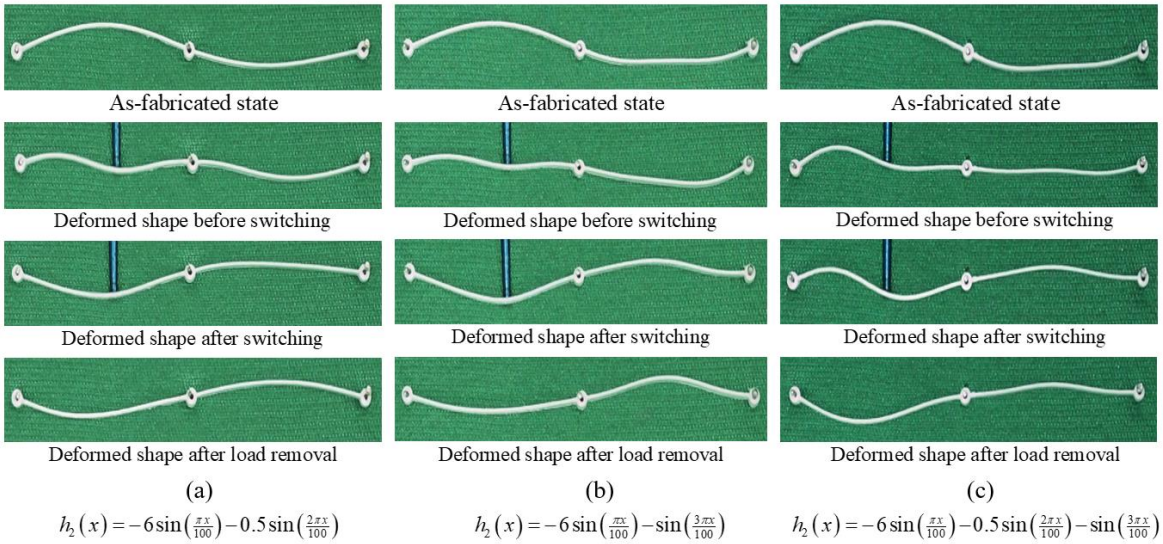

Figure 6.13: Demonstration of 3D-printed prototypes for $h_1 = 10\sin\left(\frac{\pi x}{100}\right)$.

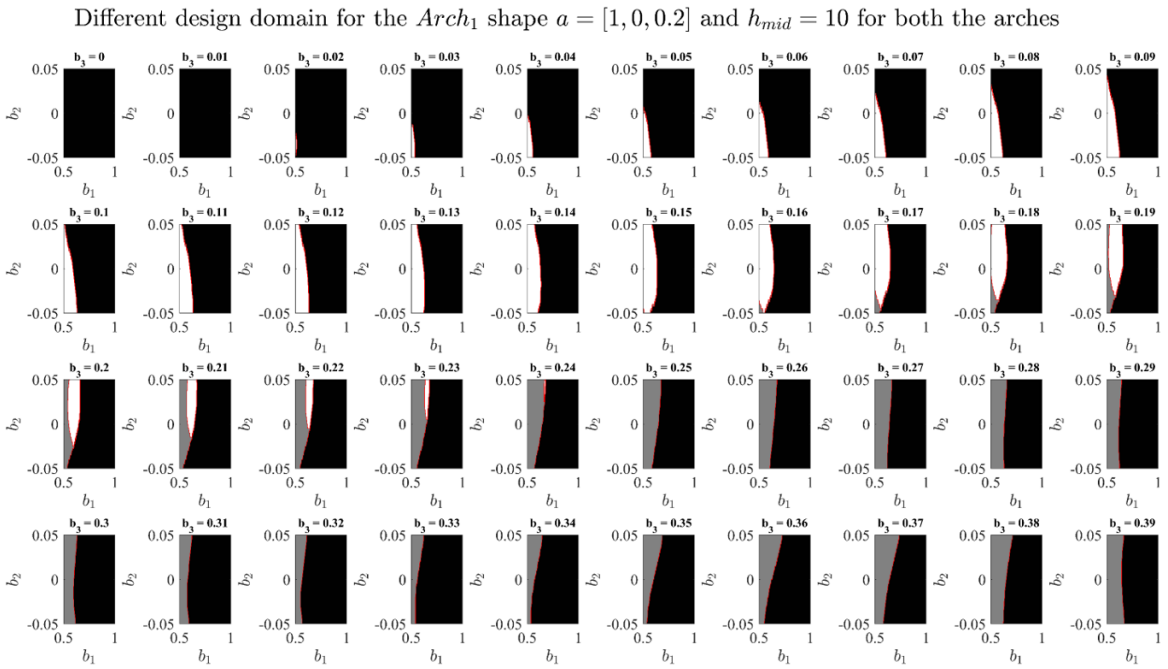

Figure 6.14: Design domain for the $Arch_1$ shape $a = [1, 0, 0.2]$. The black color region indicates the *not-switching and not-bistable* (NSNB) domain, the grey indicates the s*witching and not-bistable* (SNB) domain, and the white indicates the *switching and bistable* (SB) domain. h_{mid} is taken to be 10 for both the cases.

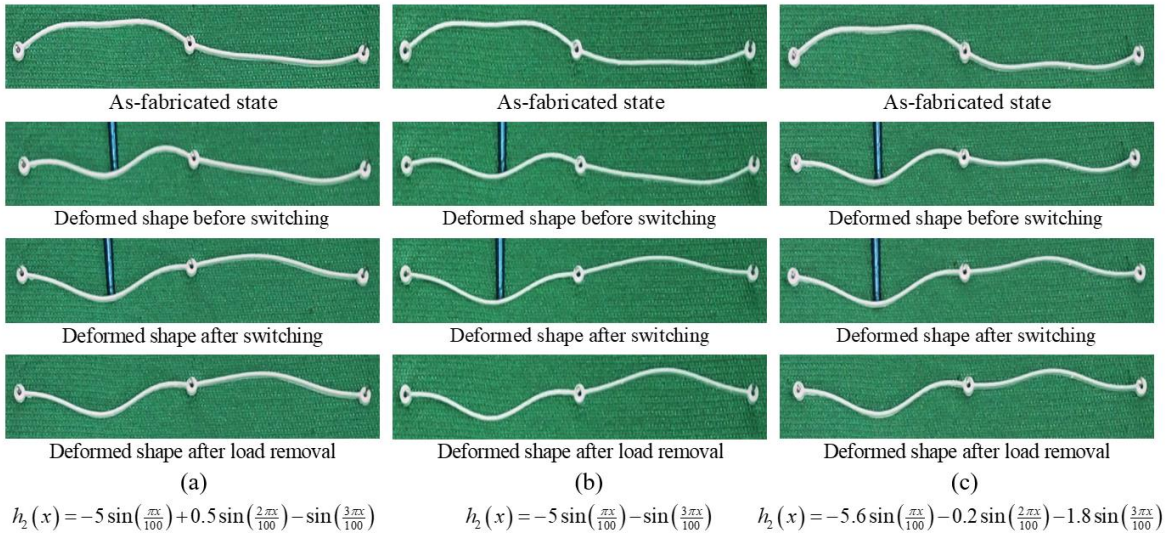

Figure 6.15: Demonstration of 3D-printed prototypes for $h_1 = 110\sin\left(\frac{\pi x}{100}\right) + 2\sin\left(\frac{3\pi x}{100}\right)$.

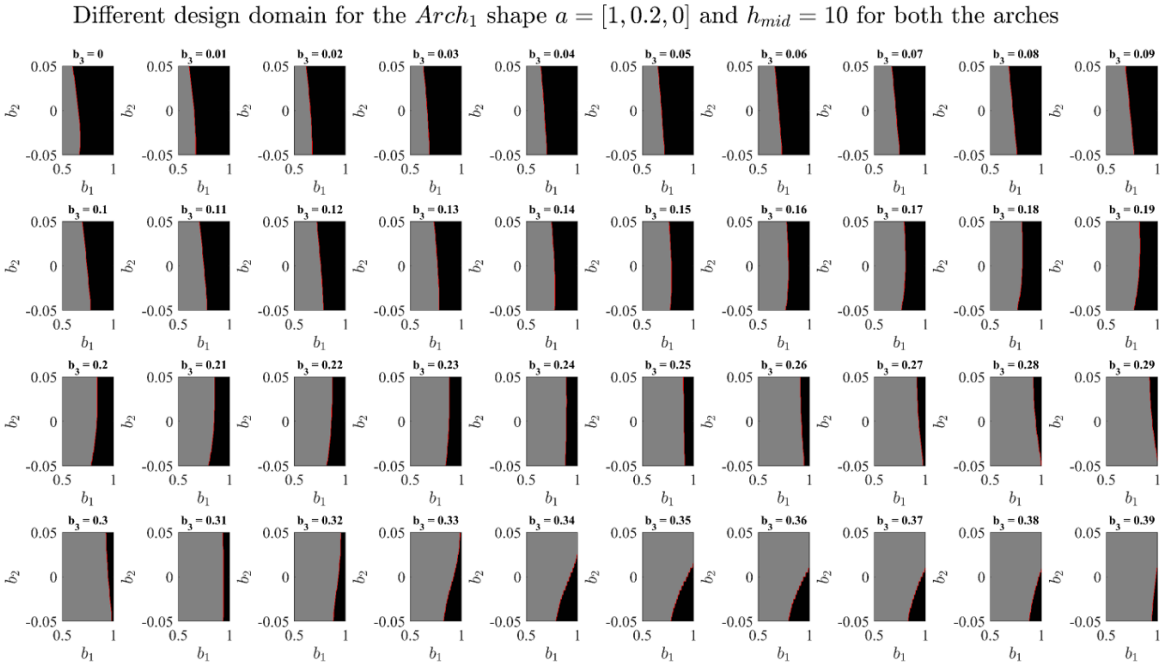

Figure 6.16: Design domain for the $Arch_1$ shape $a = [1, 0.2, 0]$. The black color region indicates the *not-switching and not-bistable* (NSNB) domain, and the grey indicates the s*witching and not-bistable* (SNB) domain. h_{mid} is taken to be 10 for both the cases.

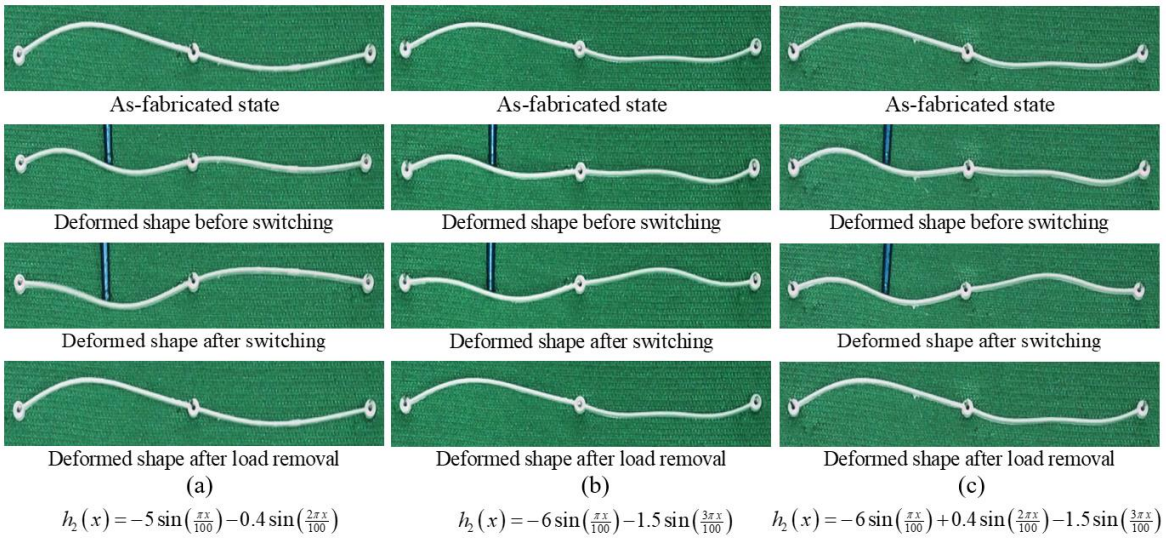

Figure 6.17: Demonstration of 3D-printed prototypes for $h_1 = 110\sin\left(\frac{\pi x}{100}\right) + 2\sin\left(\frac{2\pi x}{100}\right)$.

6.9 Closure

In this chapter, we have introduced connected arches and obtained the governing equations to analyse them. Based on the flipping of the second arch and their stability at the inverted shape, we catagorize them into four broad groups. We derived the flipping and the bistability conditions for these connected arches, which can be used to predict the nature of the connected arch for any arbitrary $Arch_1$ and $Arch_2$ shapes. This will be helpful in choosing arch geometry for various applications which will be discussed in Chapter 8. In the next chapter we obtain a bilateral relationship between the two stable state configurations of connected arch.